

Temperature-induced phase transition and Li self-diffusion in Li_2C_2 : A first-principles study

Stanislav Filippov,^{1,2} Johan Klarbring,¹ Ulrich Häussermann,² and Sergei I. Simak¹

¹*Department of Physics, Chemistry, and Biology (IFM), Linköping University, SE-581 83 Linköping, Sweden*

²*Department of Materials and Environmental Chemistry, Stockholm University, SE-10691 Stockholm, Sweden*



(Received 24 September 2018; revised manuscript received 19 December 2018; published 19 February 2019)

Lithium carbide, Li_2C_2 , is a fascinating material that combines strong covalent and weak ionic bonding resulting in a wide range of unusual properties. The mechanism of its phase transition from the ground-state orthorhombic ($Immm$) to the high-temperature cubic ($Fm\bar{3}m$) crystal structure is not well understood and here we elucidate it with help of first-principles calculations. We show that stabilization of the cubic phase is a result of a temperature-induced disorientation of the C-C dumbbells and their further thermal rotations. Due to these rotations rather large deviatoric stress, which is associated with the dumbbell alignment along one of the crystallographic axes, averages out making the cubic structure mechanically stable. At high temperature we observe a type-II superionic transition to a state of high Li self-diffusion involving collective ionic motion mediated by the formation of Frenkel pairs.

DOI: [10.1103/PhysRevMaterials.3.023602](https://doi.org/10.1103/PhysRevMaterials.3.023602)

I. INTRODUCTION

Carbides of alkali (A) and alkaline earth metals (Ae)— A_2C_2 and AeC_2 , respectively—occur predominantly as salt-like acetylides that consist of the C_2 -dumbbell anion isoelectronic to dinitrogen with a strong triple bond [1]. Achieving optimum mutual coordination of dumbbells and cations in a crystal structure seems to be delicate as most acetylide carbides exhibit polymorphism [2–7]. Structural variety arises from differently oriented dumbbell units which are embedded in a distorted octahedral or cubelike environment of metal atoms in crystal structures that relate to the NaCl (for AeC_2 , alkaline earth metal $\text{Ae} = \text{Ca}–\text{Ba}$) and anti- CaF_2 (for A_2C_2 , alkaline metal $\text{A} = \text{Li}–\text{K}$) type structures. With increasing temperature, C_2 dumbbells develop orientational disorder and acetylide carbides transform to high temperature modifications in which the metal atoms attain a high symmetry cubic partial structure. The polymorphism of dumbbell-ordered acetylide carbides, the mechanism of the temperature induced order-disorder phase transition, and the nature of disorder in the high temperature phase (i.e., static vs dynamic) are not well understood. A previous investigation of K_2C_2 using powder x-ray diffraction (PXRD) and C^{13} nuclear magnetic resonance (NMR) spectroscopy revealed dynamically disordered dumbbell moieties in the high temperature phase, stable above 420 K. It was however not possible to discern whether the dynamics of C_2 units corresponded to free rotation or fast reorientations [8].

In this work we investigate Li_2C_2 whose orthorhombic ground state crystal structure is portrayed in Fig. 1. It features C_2 dumbbells oriented along the crystallographic \mathbf{b} direction. The dumbbells are coordinated by 8 Li atoms (or rather ions) in a distorted cubelike fashion. Dumbbells are oriented along diagonally opposite edges in the distorted cube environment, which is pronouncedly elongated in the direction of the dumbbell. Li_2C_2 can be conveniently prepared from the elements. Although the compound was already reported in 1896 [9] it

was not before recently that interesting materials properties and potential technological applications could be associated with Li_2C_2 . These include the application of Li_2C_2 as cathode material in Li ion batteries [10–12], and its occurrence as intermediate of Li_2CO_3 reduction in the solid-electrolyte interphase layer on the anode of Li batteries [13]. Further, it has been shown that Li can be removed from Li_2C_2 in mild oxidation reactions leading to nanopatterned carbon [14] and it has been predicted that Li_2C_2 represents a precursor toward novel metallic and superconducting polycarbides [15,16]. This was recently partially confirmed by experiments that indicated an irreversible polymerization of C_2 units when pressurizing Li_2C_2 to around 50 GPa [17].

As established from differential thermal analysis experiments, Li_2C_2 displays a high temperature phase transition near 698 K (425 °C) [18–20] and melts at around 1323 K (1050 °C) [19]. The transformation from the low temperature (LT) $Immm$ ground state phase (cf. Fig. 1) to the cubic high-temperature (HT) phase was then explicitly shown in a multitemperature PXRD experiment by Ruschewitz and Pöttgen [20]. Noteworthy is the sluggish character of the phase transition, showing LT and HT phase simultaneously present over a temperature range exceeding 100 K. The structure of the HT phase corresponds to the anti- CaF_2 type structure with orientationally disordered C_2 dumbbells attaining a face-centered cubic (fcc) arrangement (with respect to their centers of gravity) and Li atoms situated in the tetrahedral voids (forming a simple cubic partial structure). The relation between the LT and HT structure is depicted in Fig. 2. Figure 2(a) presents a larger segment of the LT structure in which besides the conventional I-centered orthorhombic unit cell an F-centered monoclinic unit cell—relating to the F-centered cubic unit cell of the HT phase—is included. *Vice versa*, Fig. 2(b) shows the corresponding structural segment for the HT phase. Here, besides the conventional cubic unit cell also an I-centered tetragonal cell—relating to the conventional unit cell of the LT phase—is included. The disordered C_2

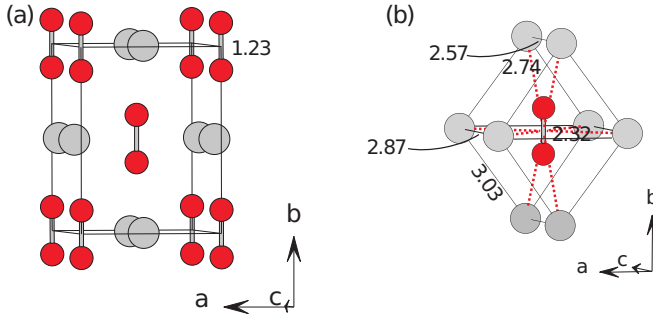


FIG. 1. Conventional representation of the *Immm* ground state structure of Li_2C_2 (a) and the coordination of a C_2 dumbbell by 8 Li (b). Li and C atoms are shown as gray and red circles, respectively. Selected interatomic distances are given in Å.

dumbbells are represented as assuming different orientations along the high symmetry directions $\langle 100 \rangle$, $\langle 110 \rangle$, and $\langle 111 \rangle$ in the cubic structure [Fig. 2(d)]. We note that the cubic symmetry of *Fm* $\bar{3}$ *m* is maintained in a static supercell of limited size only when the centers of mass of the dumbbells are taken into account instead of the whole dumbbells, i.e., the way the high-temperature phase is identified experimentally in Ref. [20]. In the simulations, specific orientations of the dumbbells leads to formally noncubic symmetry. However, we will refer to such structures as HT in line with Ref. [20].

It is clear that a deeper understanding of the materials properties and reactivity of Li_2C_2 will require detailed knowledge of its dynamical properties, which in turn may also give valuable insight into the puzzling polymorphism and order-disorder phase transition of acetylide carbides in general. To gain this knowledge we employed *ab initio* molecular dynamics (AIMD) covering a wide range of temperatures and addressing atomic motion in its full complexity. In the following sections the mechanism of the phase transition from the ground-state orthorhombic (*Immm*) to the high-temperature cubic (*Fm* $\bar{3}$ *m*) crystal structure is elucidated and understood. The details of the methodology are given in Sec. II and the results and discussion are provided in Sec. III.

II. METHODS

The calculations were performed by means of the density functional theory (DFT) within the generalized gradient approximation (GGA) with the Perdew-Burke-Ernzerhof (PBE) form of the exchange and correlation [21,22]. The Vienna Ab Initio Simulation Package (VASP) [23–26] employing the projector-augmented wave (PAW) method [27,28] was used. The AIMD simulations of cubic Li_2C_2 in the *NVT* ensemble (i.e., maintaining the number of atoms N , volume of the system V , and temperature T) were performed using the Nosé-Hoover thermostat at temperatures of 300, 500, 625, 750, 875, 1000, and 1200 K, all at zero pressure. The simulation cell was selected to be the $2 \times 2 \times 2$ 128 atom supercell (SC) of the conventional unit cell of the HT phase. The Brillouin zone integration was done on a $2 \times 2 \times 2$ Monkhorst-Pack (MP) k -point mesh. The orthorhombic phase was also simulated in the *NPT* ensemble (i.e., maintaining N , pressure P , and T), using the algorithm by Parrinello and Rahman [29,30],

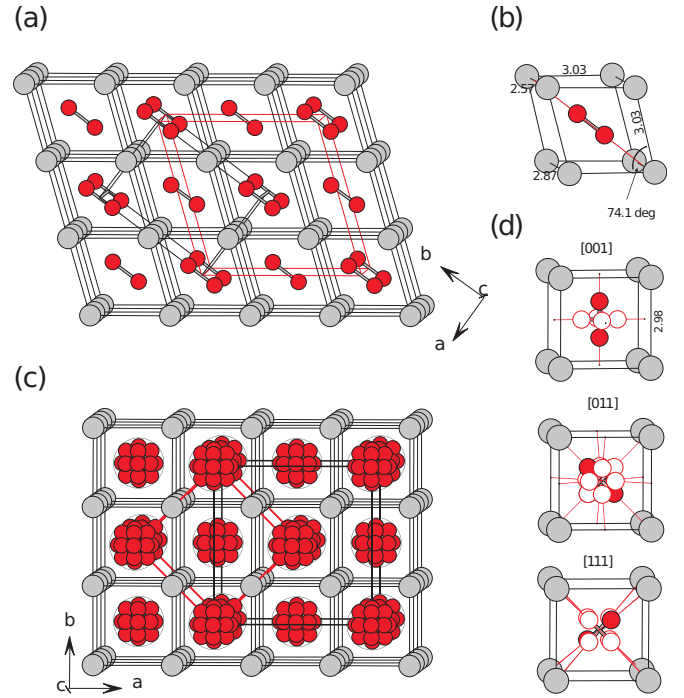


FIG. 2. Relation between LT and HT Li_2C_2 phases. Li and C atoms are shown as gray and red circles, respectively. (a) *Immm* structure with the conventional orthorhombic body (I) centered (black lines) and a monoclinic face (F) centered (red lines) unit cell (the latter relates to the cubic HT structure); (b) coordination of a C_2 dumbbell by 8 Li [as in Fig. 1(b)]; (c) cubic HT structure with F-centered (black lines) and tetragonal I-centered (red lines) unit cells (the latter relates to the LT structure). The disordered C_2 dumbbells are represented as oriented along high symmetry directions [see (d)]; (d) from top to bottom: orientations of disordered dumbbells along the high symmetry crystallographic directions $\langle 100 \rangle$ (three possible orientations, i.e., $[001]$, $[010]$, $[100]$), $\langle 110 \rangle$ (six orientations), and $\langle 111 \rangle$ (four orientations). One orientation each is emphasized by a dumbbell with filled red circles, whereas the remaining ones are indicated by open circles. Selected Li-Li distances are given in Å.

at temperatures 300, 700, 875, 1000, and 1200 K. In these simulations the temperature was controlled by a Langevin thermostat with friction coefficients of 2 ps^{-1} for each atom and 10 ps^{-1} for the lattice degrees of freedom, following suggestions of Ref. [31]. The fictitious mass of lattice degrees of freedom was set to 2 amu [31]. These parameters were checked against stability of an *Immm* SC at 300 K. The SC was chosen to be a $2 \times 2 \times 2$ repetition of the conventional orthorhombic unit cell (see Fig. 1) and contained 64 atoms. The crystallographic connection between the cubic and orthorhombic phases is depicted in Fig. 2(b). The MP k -point mesh was chosen to be $3 \times 3 \times 3$ to account for the SC size. In these simulations, the energies of the electronic self-consistent iterations were converged to less than 10^{-5} eV . The time step in all the MD simulations was set to 1 fs. The total number of time steps was in the range 20 000 to 40 000.

The phonon dispersions at 0 K were calculated within the small displacement method [32,33] as implemented in the Phonopy package (v. 1.11.12) [34]. The calculations were performed for both cubic and orthorhombic structures with

TABLE I. Cubic HT phase. Calculated values of minimum total energy, volume minimizing the energy, and deviatoric diagonal [$\delta_{ii} = \sigma_{ii} - P$, $P = \text{tr}(\sigma)/3$] and nondiagonal components of the stress tensor at the corresponding volume for different static alignments of dumbbells at 0 K.

C ₂ align.	Energy (eV/at.)	Vol. (Å ³ /at.)	Stresses (GPa)					
			δ_{xx}	δ_{yy}	δ_{zz}	σ_{xy}	σ_{yz}	σ_{zx}
[001]	-5.452	12.63	-3.12	-3.12	3.97	0.00	0.00	0.00
[111]	-5.446	12.92	0.00	0.00	0.00	4.88	4.88	4.88
[011]	-5.393	14.02	-7.11	2.09	2.09	0.00	9.11	0.00

108 atoms in a $3 \times 3 \times 3$ SC built from primitive cells, on the $4 \times 4 \times 4$ k -point MP mesh. The displacements were selected to be 0.03 Å that provides a reasonable balance between a sufficiently small size of the displacement to stay in a linear force-displacement regime and large enough forces to reduce numerical errors. To get accurate forces, the energies of the electronic self-consistent iterations in phonon calculations were converged to less than 10^{-8} eV. The cutoff energy for the plane-wave expansion was set to 675 eV in all the calculations, similar to Ref. [35].

Probability density plots of the angular distribution of the C₂ dumbbells were obtained by binning the inclination and azimuthal angle of each dumbbell at each time step of the AIMD simulation into a 2D histogram. Since a uniform distribution in the inclination-azimuth plane is not uniform on the sphere, the distribution was normalized with respect to a distribution that is uniform on the sphere before producing the plots of Figs. 5 and 8. Both the vectors from the first to the second and from the second to the first of two C atoms making up a dumbbell were used, in order for a single dumbbell to give a signal on both sides of the sphere.

III. RESULTS AND DISCUSSION

A. Static calculations

As we noted earlier, the cubic symmetry of Li₂C₂ is retained only with respect to the centers of gravity of the C-C dumbbells. This is exactly the case of the experimental structural characterizations like x-ray diffraction (XRD), where only the time-averaged atomic positions are revealed. In actual simulations we need, of course, to explicitly specify the positions of the C atoms. Table I summarizes calculations of total energy, equilibrium volume, deviatoric stress, and nondiagonal components of the stress tensor obtained at the equilibrium volume for the cases when all the dumbbells are oriented along the [001], [011], or [111] high symmetry directions of the HT phase. The minimum energies of the structures with [001] and [111] oriented dumbbells are very similar, with a difference of approximately 6 meV/atom. The structure with the alignment along [011], however, lies much higher in energy (by ≈ 60 meV/atom). It is worth noting that according to Table I all these structures are subject to nonzero stress at the volume minimizing the energy and therefore the total energy differences in Table I may play a less important role than the ability of the system to release the stress by

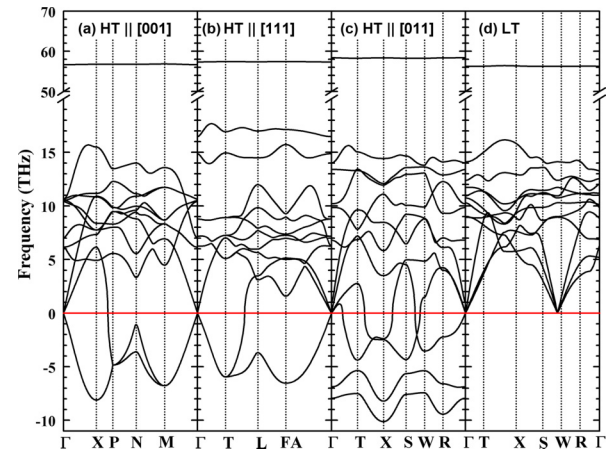


FIG. 3. Phonon dispersions calculated at 0 K for (a) HT phase with the dumbbells oriented along [001], (b) HT phase with the dumbbells oriented along [111], (c) HT phase with the dumbbells oriented along [011], and (d) orthorhombic phase.

allowing the thermal movement of atoms. We discuss this later in more detail.

Calculated phonon dispersions for the low-energy HT structures (with the C₂ dumbbells oriented along the [001], [111], and [011] directions) as well as the orthorhombic phases are shown in Fig. 3. Certainly, the HT phase does not exist at 0 K. It belongs to cubic ($Fm\bar{3}m$) space group and can do so only when just the centers of gravity of the dumbbells are considered. With any fixed ordered orientation of the C₂ dumbbells the actual symmetry lowers. Particularly, the HT phase with dumbbells oriented along [001] has actual $I4/mmm$ space group symmetry, orientation of all the dumbbells along [111] results in $R\bar{3}m$ symmetry, and with their [011] orientation the space group becomes $Immm$. In fact the latter orientation corresponds to the distorted LT phase; cf. Fig. 2. Such atomic arrangements should be out of the equilibrium and therefore unfavorable, as seen from Table I. Nevertheless, some important peculiarities can be analyzed. In particular, one may see that the dispersion relations for all these phases with fixed directions of the carbon dumbbells have a common feature: the strongly localized high-frequency modes around 56 THz (1868 cm^{-1}). This matches the value of the A_{1g} Raman mode measured at 1864 cm^{-1} that corresponds to the C-C stretching mode [36]. The pronounced localization of the modes with a high characteristic frequency is typical of a strong covalent bond between the carbon atoms and of molecules embedded into or adsorbed on a surface of solids.

Further, the orthorhombic LT phase shows no imaginary modes and is therefore dynamically stable at low temperatures, in agreement with the experimental findings [20]. On the contrary, the HT structures show acoustic imaginary modes for the dumbbell orientation along [001] and [111]. The HT phase with C₂ dumbbells orientation along [011] demonstrates both acoustic and optical imaginary modes. The latter is not surprising since this structure is in fact a distorted variant of the LT phase. This underlines that the HT structure is dynamically unstable for any collinearly ordered static orientation of the dumbbells at 0 K.

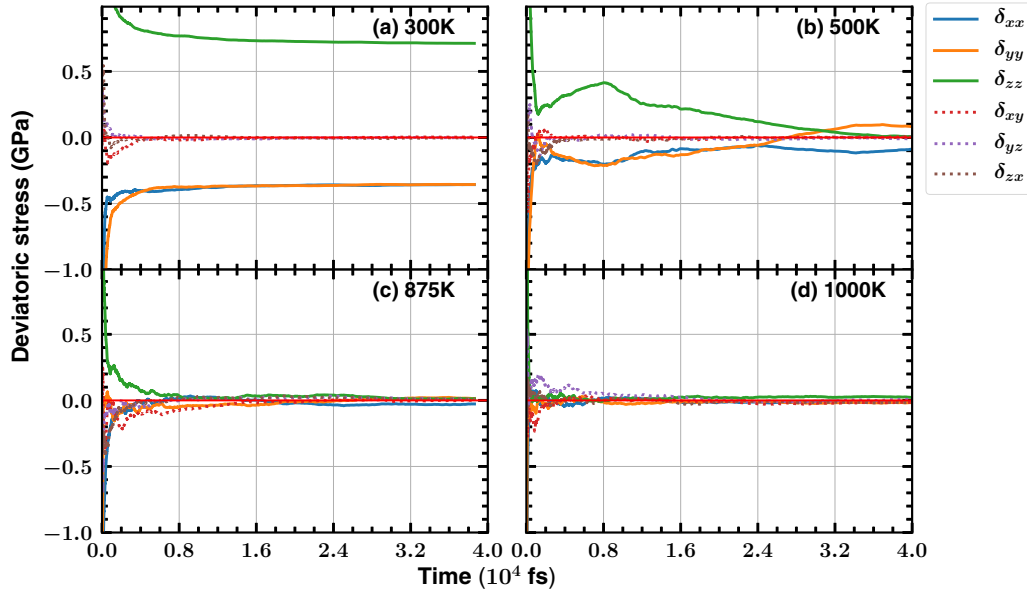


FIG. 4. Deviatoric stress $\delta_{ii} = \sigma_{ii} - P$, $P = \text{tr}(\sigma)/3$, $\delta_{ij} = \sigma_{ij}$, if $i \neq j$, as a function of the simulation time for various temperatures in the “cubic” structure. The presented data correspond to the volumes that provide the smallest values of the deviatoric stress. The red horizontal line represents the zero deviatoric stress. The figure also shows the nondiagonal components of the stress tensor.

Table I shows the deviatoric diagonal and nondiagonal components of the stress tensor for the HT phase for the different orientations of the C_2 dumbbells calculated at volumes minimizing the total energy for a particular static alignment of the dumbbells. In the case of the [001] alignment, σ_{zz} exceeds the other diagonal components, σ_{xx} and σ_{yy} , while the nondiagonal components are practically zero. When the carbon dumbbells are aligned along [011], i.e., in the $YZ((100))$ plane, only σ_{yz} becomes large. If the dumbbells are aligned along [111], all nondiagonal components attain similar large values that are comparable to the diagonal ones. In addition to that, the diagonal stress components become nearly equal. This behavior can be explained under the assumption that there is a contribution to tensile stress associated with each dumbbell in the case of their static orientations that tends to distort the cubic shape of the crystal. This force contributes to the stress tensor and this contribution can be regarded as projections of this force on the corresponding crystallographic directions and planes. Indeed, when the dumbbells are oriented along [001] (i.e., the Z axis), only σ_{zz} becomes larger than one-third of the trace of the stress components that formally defines pressure. In the case of the [011] orientation, i.e., when the dumbbells are in the $YZ((100))$ plane, σ_{yy} and σ_{zz} are equal, and the nondiagonal component σ_{yz} takes a nonzero value. When the dumbbells are oriented along [111], the diagonal components share the same values as well as the nondiagonal ones, since [111] makes the same angles between all the coordinate planes [ZX , i.e., (010), XY , i.e., (001), and YZ , i.e., (100)] and the axes. Thus it is natural to expect that the high-temperature stabilization of the HT structure should involve motion of the carbon dumbbells.

B. MD simulations – C_2 disorder

As the starting point of our NVT AIMD simulations we used the HT structure with the lowest energy configuration

(i.e., the [001] orientation of dumbbells). As follows from the discussion above, we expect zeroing of the deviatoric stress by the thermal disorientation that will remove any preferential orientation of the C_2 dumbbells even if the structure was initialized with the preferential orientation along [001]. Figure 4 shows deviatoric stresses calculated for several temperatures as a function of simulation time. At 300 K δ_{zz} is much larger than $\delta_{xx} = \delta_{yy}$ [Fig. 4(a)]. As the simulation temperature increases, the deviatoric stress converges to zero; see Figs. 4(b)–4(d). This correlates with a thermal disorientation of the C_2 dumbbells as seen in Fig. 5. The fact that the stresses are equalized at high temperature indicates that the thermal disorder of the C_2 dumbbells might indeed be an important mechanism of stabilization of the HT phase.

The thermal disorder of the C-C dumbbells in the cubic HT phase is not unique to Li_2C_2 , but occurs in several alkali acetylides. In particular, such disorder was studied experimentally in K_2C_2 [8]. However, the methodology used in Ref. [8] did not allow the authors to discriminate among several possible models as follows.

- (i) The Pauling model (dynamic disorder with isotropic free rotation of the C_2 dumbbells).
- (ii) The Frenkel model (dynamic disorder with a random jumps between different orientations of the dumbbells along high symmetry directions, e.g., [001], [110], etc.).
- (iii) Static disorder with a random orientation of dumbbells.
- (iv) Static disorder with the dumbbells oriented along high symmetry directions of the cubic crystal.

AIMD simulations allow one to address such an issue directly. Figure 5 shows 3D density plots of angular distribution of orientations of the C-C dumbbells. At 300 K the dumbbells orient in the XZ and YZ planes in symmetrically equivalent positions with inclination angle (i.e., angle between [001] and the dumbbell’s axis) of 55° . With further increase of temperature, the dumbbells tend to align predominantly along

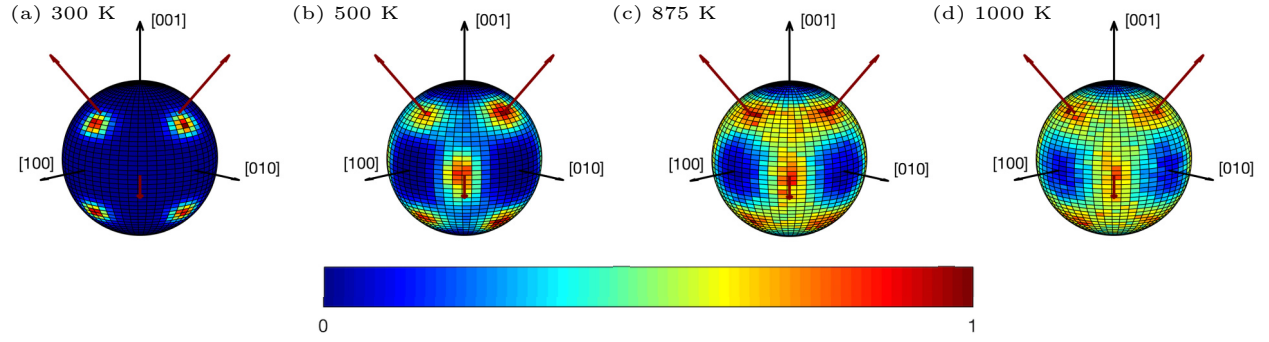


FIG. 5. Probability density plots of angular positions of the C-C dumbbells under various temperatures. The plots represent results of averaging over the ensemble. The blue color corresponds to the lowest probability, while red corresponds to the maximal probability of observation of the pairs. The red arrows point in the $[110]$, $[011]$, and $[101]$ directions.

$\langle 011 \rangle$ directions, with increasing coverage of the space of possible angular positions around these directions. The plots in Figs. 5(b)–5(d) indicate that C_2 dumbbells might perform jumps between $\langle 011 \rangle$ directions. Obviously, as it is seen from Figs. 5(b)–5(d), the higher the temperature the higher the probability of such jumps.

The plots in Fig. 5 are, however, unable to reveal the presence of any correlations in the C_2 dynamics. To address this issue, we define correlation functions:

$$c_\beta(t) = \frac{1}{N_{C_2}} \sum_{\alpha=1}^{N_{C_2}} \frac{1}{N_\beta} \sum_{i=1}^{N_\beta} \frac{|\Delta \vec{r}_\alpha(t) \cdot \Delta \vec{r}_i(t)|}{|\Delta \vec{r}_\alpha(t)| |\Delta \vec{r}_i(t)|}.$$

The vectors $\Delta \vec{r}$ are defined as $\Delta \vec{r} = \vec{r}_1 - \vec{r}_0$, where \vec{r}_1 and \vec{r}_0 are the positions of the two C atoms forming the given C_2 dumbbell. The sum is over all N_β nearest neighbors of a dumbbell α , belonging to a particular coordinate plane $\beta = XY, YZ$, or XZ ; N_{C_2} is the total number of the dumbbells in the simulation box. We stress here that the $c_\beta(t)$ defined above is essentially a cosine of the angle between two C_2 dumbbells in the first coordination shell averaged over all nearest neighbors of a given dumbbell α and then averaged over the ensemble of dumbbells. Due to the definition, the temporal evolution of $c_\beta(t)$ is important and reflects the presence or absence of correlations. Indeed, in case of a random process $c_\beta(t)$ takes randomly any value between zero and 1, while for a correlation over a period of time, $c_\beta(t)$ keeps approximately the same value. The correlation functions at temperatures 300, 500, and 1000 K are shown in Fig. 6.

If the alignment of the dumbbells is correlated, the correlation function holds a roughly constant value over the time range where such correlation exists. This is exactly the case of Fig. 6(a) plotted for 300 K. At this temperature, the dumbbells initially reorient during ~ 5000 fs and then keep the attained orientation over the rest of the simulation time. The resulting structure is shown in Fig. 7(a). In this structure dumbbells are tilted with respect to their starting configuration. Interestingly, this structure appears to be composed of slabs of orthorhombic LT structure [cf. Fig. 2(a)]. These slabs are mutually rotated by 90° along the stacking direction (which is the c direction of the simulation box). Within a slab, dumbbells are oriented in the same direction. Dumbbells are embedded in an elongated cubelike environment of 8 Li atoms. Compared to the

orthorhombic LT structure Li-Li distances of the distorted cube are more regular, but similar to the LT structure the dumbbells are oriented along opposite edges in the elongation direction. It is clear that the inclination angle of 55° observed in Fig. 7(a) relates to the elongation direction of the distorted cube environment [Fig. 7(b)]. The structure with this non-collinear alignment of the carbon dumbbells that we find at 300 K turns out to be close in energy to the ground state orthorhombic structure and it is dynamically stable, i.e., the phonon dispersion relations (not presented here) do not have any imaginary frequencies.

At 500 K the Li atoms attain the regular cubelike arrangement characteristic of the HT structure. The orientation of the C_2 dumbbells is now along the $[101]$, $[110]$, and $[011]$ directions in the cubic environment. Accordingly, the inclination angle changes to 45° . The dumbbells collectively

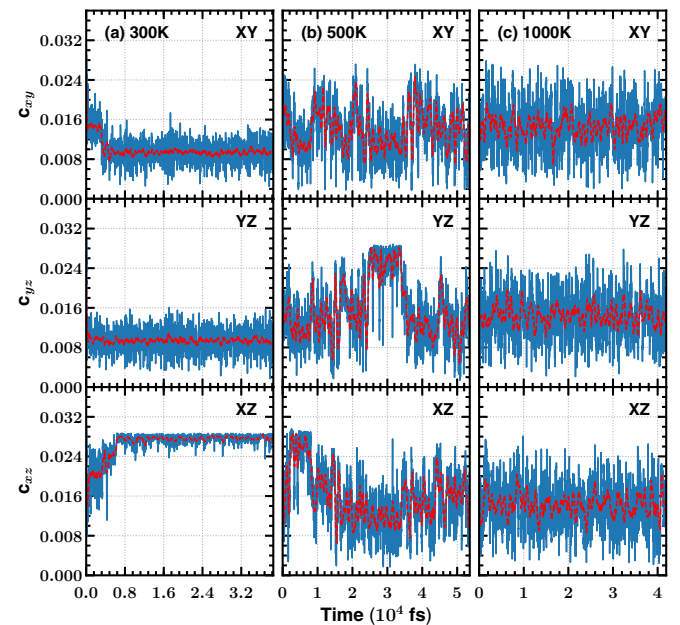


FIG. 6. Correlation functions averaged over all nearest neighbors lying in planes XY , YZ , and XZ for different temperatures. The correlation function is defined in the text. The dotted red line is a guideline.

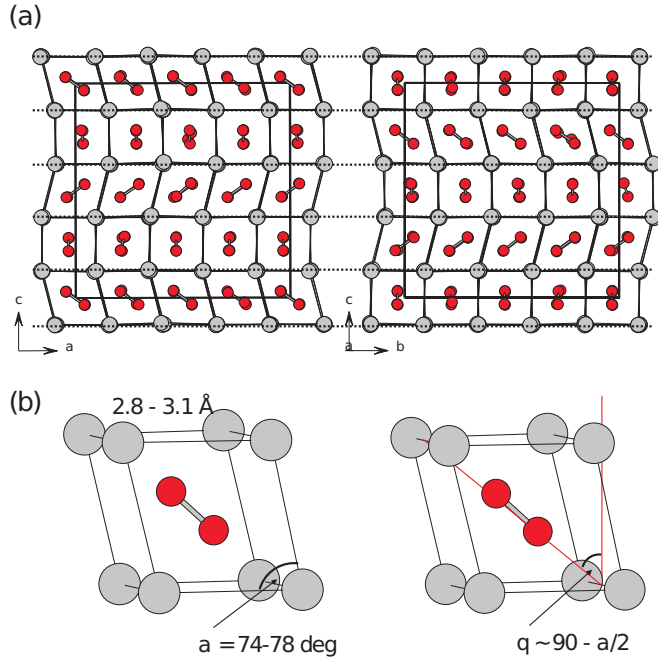


FIG. 7. (a) Average atomic positions obtained from an *NVT* simulation at 300 K. (b) The LT unit cell which builds up the layers of the structure in (a). The layers are mutually rotated by 90° along the stacking direction.

swap their positions as seen in Fig. 6(b) and the final structural arrangement corresponds to cubic HT structure with dumbbells randomly oriented along the six possible $\langle 110 \rangle$ directions (notice that the dumbbells aligned along any pair of directions, like $[110]$ and $[\bar{1}\bar{1}0]$, are identical). The situation corresponds to a transition from static to dynamic disorder, i.e., within a rather short period of time (hundreds of fs) the dumbbells keep their orientation, but then randomly swap their positions.

In the case of no correlation between the dumbbells, the correlation function takes randomly any value between zero and 1, and the corresponding plot will look like white noise. However, due to averaging over four nearest neighbors and then over all the dumbbells in the simulation box, the amplitude will be diminished [cf. Fig. 6(c)]. We observe exactly this case in Fig. 6(c) plotted for 1000 K.

In light of the described peculiarities, the stabilization of the HT phase can be understood as follows. As one could see above, there is a contribution to tensile stress associated with a dumbbell. Any static alignment of the dumbbells along a preferred direction results in large stresses tending to distort the cubic cell. Obviously such orientation is energetically unfavorable. With introduction of thermal energy into the cubic Li_2C_2 the dumbbells become mobile and will orient in a way to minimize the stress. To do that, the dumbbells should be disordered, and the structure shown in Fig. 7(a) emerges. Consequently, the deviatoric stress drops to less than 1 GPa [compare Table I and Fig. 4(a)]. When the dumbbells orient along $[110]$, $[101]$, and $[011]$ directions at 500 K, the deviatoric stress decreases even further. Finally, when the C_2 dumbbells actively jump between those orientations, the deviatoric stress becomes zero. This clearly indicates that the contribution to tensile stress of an individual dumbbell is

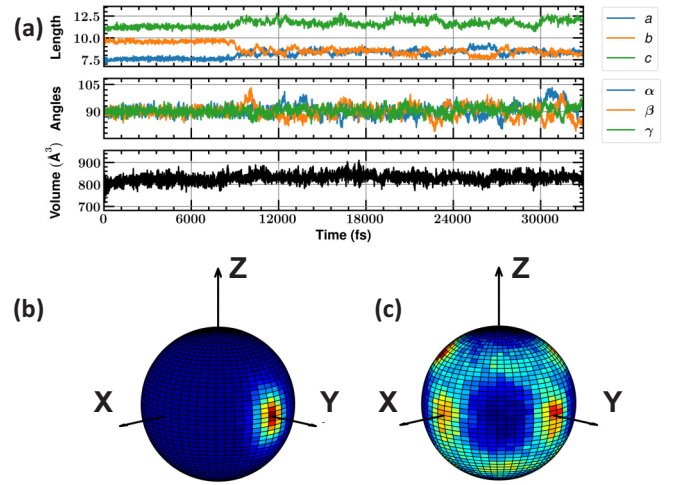


FIG. 8. Time evolution of lattice parameters of the orthorhombic SC at 700 K (a). Panels (b) and (c) represent results of averaging over the ensemble of the probability densities before and after the phase transition, respectively. Due to change of the symmetry and the shape of the simulation box, we show here Cartesian axes.

effectively averaged out due to these jumps between the equivalent positions.

The importance of the dumbbell orientations along $\langle 110 \rangle$ and consequent jumps between those directions is also clearly seen in *NPT* AIMD simulations performed on the $2 \times 2 \times 2$ orthorhombic SC. Time evolution of the lattice parameters of the simulation box is shown in Fig. 8(a) at 700 K. The angles between the lattice vectors remain 90° in the SC constructed from a conventional unit cell [see the blacklined unit cell in Fig. 2(a)] over the whole simulation time. The SC keeps the initial lattice parameters for the first 8 ps. However, after this time interval they evolve to $c/b = c/a = 1.41 \approx \sqrt{2}$, which is in fact the tetragonal representation for the cubic lattice. Therefore, the transition from the orthorhombic to cubic phase is directly obtained in our *NPT* AIMD simulation. The observed changes are accompanied by a qualitative change in dynamics of the C_2 dumbbells depicted in Fig. 8(b) and Fig. 8(c). These plots show that while before the transition the dumbbells keep their low-temperature alignment, after 8 ps they become mobile in exactly the same way as seen in Fig. 6. The corresponding volume expansion is approximately 4% with respect to the volume of the initial structure. We notice that the experimentally reported transition temperature is about 698 K, i.e., we observe the transition at a temperature rather close to this value [20]. The fact that the LT phase is present for 8 ps before the transformation to the HT phase suggests that both phases are local free energy minima at this temperature. Therefore, in a real sample, these phases might coexist as was indeed observed in Ref. [20].

We also note that previously the authors of Ref. [12] theoretically predicted this transition to happen at 1200 K, way too far from the experimental and our theoretical observations. Though Ref. [12] did not explicitly state what ensemble was used for the MD simulations, one may assume that most probably it was *NVT* rather than *NPT*. In such a case the large discrepancy can easily stem from the fixed cell shape.

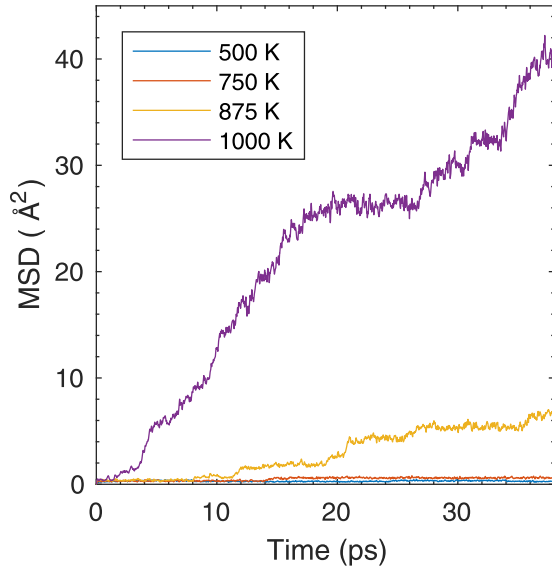


FIG. 9. MSD of the Li ions from AIMD simulations in the cubic phase at varying temperatures. Continuous diffusion, indicated by a nonzero slope of the MSD, is found for temperatures at and above 875 K.

Indeed, the key factor of this phase transition is the mobility of the C_2 dumbbells. With increase of the thermal energy of the system, they will inevitably strive to be mobile, and the only way to lower the free energy is to distort the lattice. However, in a situation of the fixed SC shape, this is impossible, so the dumbbells will be forced to be immobile. Only further increase of thermal energy will liberate the fixed dumbbells. As a result, the phase transition will be observed at much higher temperature. This example shows the power of the *NPT* AIMD to capture phase transitions in complex systems, and we think this method might be advantageous with respect to the *NVT* AIMD for such purposes. We stress here that precise identification of the transition temperature was beyond the scope of this research, and we only highlight the potential of the *NPT* simulations.

C. MD simulations – Li mobility

At high temperature, we observe substantial self-diffusion of the Li ions in the AIMD simulations of the HT phase. Figure 9 shows the mean square displacement (MSD) of the Li ions during a set of AIMD simulations at different temperatures. Continuous Li diffusion is first observed in the simulation at 875 K. We note that since there are no vacancies present in the simulation cell, the diffusion events cannot consist of isolated Li vacancy hops. As discussed above, the high-temperature cubic phase of Li_2C_2 can be viewed as an anti- CaF_2 , structure with the Li ions occupying the F positions forming a simple cubic sublattice, and the center of gravity of the thermally disordered C-C dumbbell occupying the Ca position. Most (anti-) CaF_2 structured materials undergo a so-called superionic transition to a phase characterized by a high degree of thermal disorder in the simple cubic sublattice. This disorder is mediated by the formation of Frenkel pair (FP) defects, which are, in the Li_2C_2 system,

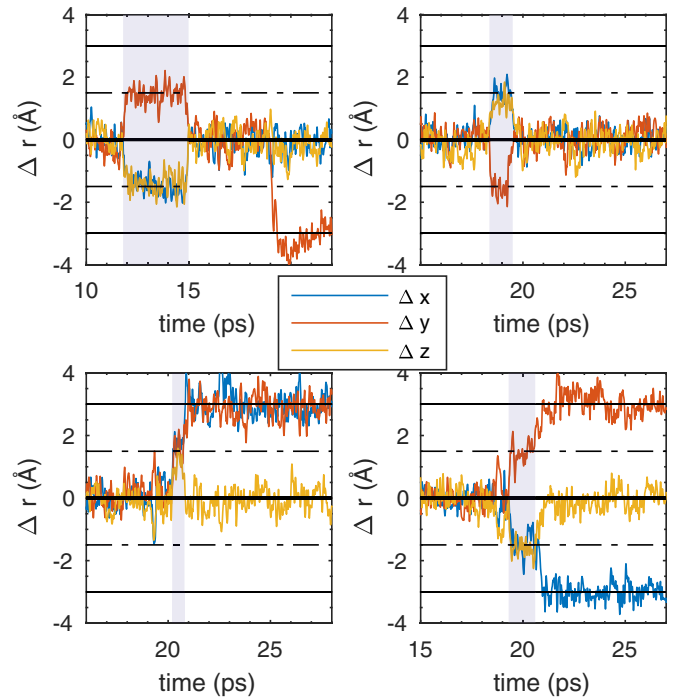


FIG. 10. Displacement in the x , y , and z direction from the ideal lattice sites in the cubic phase of four selected Li ions from an AIMD simulation at 875 K. The dashed lines correspond to the displacement distance to the octahedral interstitial position and the solid lines to the nearest neighbor ideal Li lattice site. The gray shaded areas mark the times where the particular Li ion occupies an octahedral interstitial position.

pairs of Li vacancies and interstitials. Indeed, upon a more detailed investigation of the Li ion trajectories obtained from the AIMD simulations, we observe a rapid formation and recombination of Li FPs at temperatures starting from 875 K. Figure 10 shows the displacement from the ideal starting positions, in the x , y , and z directions, of four selected Li ions during selected parts of the AIMD simulation (about 10 ps long) at 875 K. It can be clearly seen that these Li ions occupy the octahedral interstitial position of the fluorite structure during parts of the simulation. The lifetimes of these FPs vary from about 4 ps down to slightly under 1 ps. We further find, similar to what was recently found for fluorite structured CeO_2 [37], that the FPs tend to form in a collective process, where, simultaneously with the movement of one Li ion into the octahedral interstitial, another Li ion diffuses into the vacant position left behind by the first one, giving the interstitial Li ion a full eight nearest neighboring Li ions. This effectively leaves a vacant Li site in the lattice, which can promote further diffusion in the form of Li vacancy hopping. Most of these vacancy hops are found to occur in the $\langle 100 \rangle$ directions, but a few hops in the $\langle 110 \rangle$ directions are also observed.

We note that the diffusion in the LT phase was studied in Ref. [12]. However, the study focused on the LT phase, where the diffusion is found only upon creation of Li vacancies. At the same time, the Li migration in the HT phase happens even without the Li deficiency and has the character of a type-II superionic transition [37].

IV. CONCLUSIONS

The high temperature phase transition at ambient pressure between the orthorhombic $Immm$ and cubic $Fm\bar{3}m$ phases of Li_2C_2 was studied by means of first-principles calculations. We found that the major mechanism of the destabilization of the $Immm$ phase and consequent stabilization of the $Fm\bar{3}m$ one is a thermal activation of jumps of the C-C dumbbells between equivalent orientations along the $\langle 110 \rangle$ directions. Because of these jumps large σ_{zz} is averaged down to 0 GPa and prevents the cubic phase from destabilization. Therefore, the Frenkel model describes the best evolution of Li_2C_2 with temperature. The jumps of the carbon dumbbells result in an expansion of the lattice volume by approximately 4% with respect to the starting volume. We also demonstrated that *NPT* AIMD simulations allow one to observe a phase transition not accessible in *NVT* AIMD simulations. Finally, at high temperature we found pronounced Li self-diffusion involving collective ionic motion and formation of the Frenkel

pairs. This transition to a state of high diffusivity has the character of a type-II superionic transition.

ACKNOWLEDGMENTS

The support from Swedish Research Council (VR) (Project No. 2014-4750), and the Swedish Government Strategic Research Area in Materials Science on Advanced Functional Materials at Linköping University (Faculty Grant SFO-Mat-LiU No. 2009-00971) are acknowledged by S.I.S. and J.K. S.F. acknowledges the financial support from Carl Tryggers Stiftelse (CTS) för Vetenskaplig Forskning through Grant No. 16:198. U.H. acknowledges the support from Swedish Research Council (VR) (Project No. 2014-3980). The computations were performed on resources provided by the Swedish National Infrastructure for Computing (SNIC) at High Performance Computing Center North (HPC2N). The authors would like to express their sincere gratitude to Åke Sundgren from HPC2N for high quality technical support for this research.

-
- [1] U. Ruschewitz, *Coord. Chem. Rev.* **244**, 115 (2003).
 - [2] S. Konar, J. Nylén, G. Svensson, D. Bernin, M. Edén, U. Ruschewitz, and U. Häussermann, *J. Solid State Chem.* **239**, 204 (2016).
 - [3] J. Glaser, S. Dill, M. Marzini, H. A. Mayer, and H.-J. Meyer, *Z. Anorg. Allg. Chem.* **627**, 1090 (2001).
 - [4] S. Hemmersbach, B. Zibrowius, and U. Ruschewitz, *Z. Anorg. Allg. Chem.* **625**, 1440 (1999).
 - [5] V. Vohn, W. Kockelmann, and U. Ruschewitz, *J. Alloys Compd.* **284**, 132 (1999).
 - [6] V. Vohn, M. Knapp, and U. Ruschewitz, *J. Solid State Chem.* **151**, 111 (2000).
 - [7] U. Ruschewitz, P. Müller, and W. Kockelmann, *Z. Anorg. Allg. Chem.* **627**, 513 (2001).
 - [8] B. Zibrowius, C. Bähz, M. Knapp, and U. Ruschewitz, *Phys. Chem. Chem. Phys.* **6**, 5237 (2004).
 - [9] H. Moissan, *C. R. Hebd. Seances Acad. Sci.* **122**, 362 (1896).
 - [10] F. Tang, X. Song, Y. Li, H. Wang, and X. Liu, *Electrochim. Acta* **186**, 512 (2015).
 - [11] Y. Li, X. Song, F. Tang, C. Hou, J. He, H. Wang, and X. Liu, *RSC Adv.* **6**, 54256 (2016).
 - [12] N. Tian, Y. Gao, Y. Li, Z. Wang, X. Song, and L. Chen, *Angew. Chem., Int. Ed.* **55**, 644 (2016).
 - [13] N. Tian, C. Hua, Z. Wang, and L. Chen, *J. Mater. Chem. A* **3**, 14173 (2015).
 - [14] P. Simon, X. J. Feng, M. Bobnar, P. Höhn, U. Schwarz, W. Carrillo-Cabrera, M. Baitinger, and Y. Grin, *ACS Nano* **11**, 1455 (2017).
 - [15] X.-Q. Chen, C. L. Fu, and C. Franchini, *J. Phys.: Condens. Matter* **22**, 292201 (2010).
 - [16] D. Benson, Y. Li, W. Luo, R. Ahuja, G. Svensson, and U. Häussermann, *Inorg. Chem.* **52**, 6402 (2013).
 - [17] L. Wang, X. Dong, Y. Wang, H. Zheng, K. Li, X. Peng, H. K. Mao, C. Jin, Y. Meng, M. Huang, and Z. Zhao, *J. Phys. Chem. Lett.* **8**, 4241 (2017).
 - [18] V. V. Avdeev, A. P. Savchenkova, L. A. Monyakina, I. V. Nikol'skaya, and A. V. Khvostov, *J. Phys. Chem. Solids* **57**, 947 (1996).
 - [19] M. Drüe, M. Seyring, A. Kozlov, X. Song, R. Schmid-Fetzer, and M. Rettenmayr, *J. Alloys Compd.* **575**, 403 (2013).
 - [20] U. Ruschewitz and R. Pöttgen, *Z. Anorg. Allg. Chem.* **625**, 1599 (1999).
 - [21] J. P. Perdew, K. Burke, and M. Ernzerhof, *Phys. Rev. Lett.* **77**, 3865 (1996).
 - [22] J. P. Perdew, K. Burke, and M. Ernzerhof, *Phys. Rev. Lett.* **78**, 1396 (1997).
 - [23] G. Kresse and J. Hafner, *Phys. Rev. B* **47**, 558 (1993).
 - [24] G. Kresse and J. Hafner, *Phys. Rev. B* **49**, 14251 (1994).
 - [25] G. Kresse and J. Furthmüller, *Comput. Mater. Sci.* **6**, 15 (1996).
 - [26] G. Kresse and J. Furthmüller, *Phys. Rev. B* **54**, 11169 (1996).
 - [27] P. E. Blöchl, *Phys. Rev. B* **50**, 17953 (1994).
 - [28] G. Kresse and D. Joubert, *Phys. Rev. B* **59**, 1758 (1999).
 - [29] M. Parrinello and A. Rahman, *Phys. Rev. Lett.* **45**, 1196 (1980).
 - [30] M. Parrinello and A. Rahman, *J. Appl. Phys.* **52**, 7182 (1981).
 - [31] T. Bučko and F. Šimko, *J. Chem. Phys.* **144**, 064502 (2016).
 - [32] G. Kresse, J. Furthmüller, and J. Hafner, *Europhys. Lett.* **32**, 729 (1995).
 - [33] K. Parlinski, Z. Q. Li, and Y. Kawazoe, *Phys. Rev. Lett.* **78**, 4063 (1997).
 - [34] A. Togo and I. Tanaka, *Scr. Mater.* **108**, 1 (2015).
 - [35] I. Efthimiopoulos, D. E. Benson, S. Konar, J. Nylén, G. Svensson, U. Häussermann, S. Liebig, U. Ruschewitz, G. V. Vazhenin, I. Loa, M. Hanfland, and K. Syassen, *Phys. Rev. B* **92**, 064111 (2015).
 - [36] J. Nylén, S. Konar, P. Lazor, D. Benson, and U. Häussermann, *J. Chem. Phys.* **137**, 224507 (2012).
 - [37] J. Klarbring, N. V. Skorodumova, and S. I. Simak, *Phys. Rev. B* **97**, 104309 (2018).